AKARI Deep Field South: spectroscopic observations of infrared sources

Journal Item

Publications of the Korean Astronomical Society
32: 281 ∼ 285, 2017 March

pISSN 1225-1534
eISSN 2287-6936
https://doi.org/10.5303/PKAS.2017.32.1.281

AKARI DEEP FIELD SOUTH: SPECTROSCOPIC OBSERVATIONS OF INFRARED SOURCES

Chris Sedgwick[1], Stephen Serjeant[1], Chris Pearson[2,1], Shuji Matsuura[3], Mai Shirahata[4], Hideo Matsuhara[3], Lucia Marchetti[1], Glenn J. White[1,2], Mattia Vaccari[5], Ivano Baronchelli[6], Giulia Rodighiero[6], Bunyo Hadsukade[4], David L. Clements[7], and Simon Amber[1]

[1]The Open University
[2]RAL Space, Rutherford Appleton Laboratory
[3]Institute of Space and Astronautical Science, JAXA
[4]National Astronomical Observatory of Japan
[5]Astrophysics Group, Physics Department, University of the Western Cape
[6]Dipartimento di Fisica e Astronomia, Universita degli Studi di Padova
[7]Astrophysics Group, Imperial College,Blackett Laboratory

E-mail: christopher.sedgwick@open.ac.uk

(Received June 2, 2015; Revised October 25, 2016; Accepted October 25, 2016)

ABSTRACT

We present a summary of our spectroscopic redshift catalogue of 404 sources in the *AKARI* Deep Field South (ADF-S). We have used the AAOmega spectrograph to target mid-infrared and far-infrared sources selected primarily from *AKARI* observations in this field for which we were able to obtain optical counterparts. Our sources with identified redshifts include 316 with Hα detections at $z \leq 0.345$ and 15 sources at $z > 1$ with MgII or Lyα emission lines. About 13% of our $z \leq 0.345$ sources are dominated by active galactic nuclei (AGN) emission, although many show emission from both star formation and AGNs. The median Balmer decrement is 5.9. Ultra-luminous infrared galaxies (ULIRGs) were found only in the higher-redshift sources. Optical and near infrared data will be available shortly, enabling calibration of the line luminosities and spectral energy distribution (SED) fitting for these sources.

Key words: cosmology:observations; galaxies:evolution; galaxies:active; infrared:galaxies

1. INTRODUCTION

The *AKARI* Deep Field South (ADF-S) is located close to the South Ecliptic Pole and has the advantage of very low cirrus and zodiacal dust, which makes it an ideal field for extragalactic observations. The original field was observed by the *AKARI Space Telescope* (Murakami et al. 2007) in the far-infrared (Matsuhara et al. 2006; Matsuura et al. 2011) and covered a rectangular area of ∼12 deg^2 centred on RA 04 44 00, Dec -53 20 00 (J2000).

We will describe the results of an AAOmega spectroscopy campaign using targets chosen primarily from the *AKARI* catalogues in the central 3.14 deg^2 of this field from which we have identified redshifts for 404 sources. Multi-wavelength observations made in this field will be available shortly enabling spectral energy distributions (SEDs) to be fitted to these sources.

2. METHODS: AAOMEGA SPECTROSCOPY

2.1. *Choice of targets*

Our targets were chosen primarily from sources in three *AKARI* catalogues: the 90 μm catalogue of *AKARI*'s Far-Infrared Surveyor (FIS; Kawada et al. 2007) and the 15 μm and 24 μm catalogues of *AKARI*'s InfraRed Camera (IRC; Onaka et al. 2007). We also chose targets from submillimetre catalogues ASTE/AzTEC (Hatsukade et al. 2011) at 1100 μm and the Balloon-borne Large Aperture Submillimeter Telescope (BLAST; Valiante et al. 2010) at 250, 350 and 500 μm.

Sources were targeted only where we could find opti-

Table 1
Summary of results of spectroscopic observations with AAOmega in the ADF-S. Inactive fibres include pointings for guide stars and the blank sky and unused fibres.

Run	Observation date	Exposure time hr:m:s	Active fibres	Redshifts $z \leq 0.345$ Hα range	Redshifts $0.345 < z \leq 1.0$ [OIII]/Hβ range	Redshifts $1.0 < z$ MgII or Lyα	Total Redshifts
1	29 Oct 2007	2:30:00	262	115	32	9	156
2	30 Nov 2007	1:23:40	291	52	15	1	68
3	3 Jan 2008	2:00:00	316	44	33	3	80
4	27 Nov 2008(a)	1:46:40	352	75	5	3	83
5	27 Nov 2008(b)	0:26:40	271	63	2	1	66
Multiple detections				-33	-14	-2	-49
Total			1,492	316	73	15	404

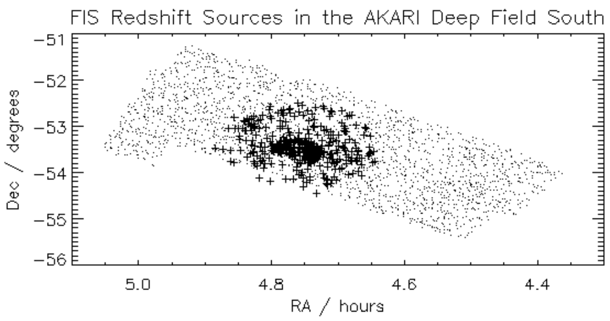

Figure 1. All AKARI-FIS sources in the ADF-S (black dots) over-plotted with spectroscopic redshift sources (plus symbols).

cal counterparts. We used the Bj-band APM catalogue for optical cross-matching of the chosen sources, and optical identifications were then checked to R-band images from the Digitised Sky Survey (DSS) and (where available) images from the CTIO 4m telescope. For our targets, we used a sparse sample based on the AAOmega fibre configuration. The area covered was π degrees (one AAOmega field-of-view). Most of the cross-identified optical sources were point sources, 94% of which fell within $10''$, and all of which fell within $16''$of the *AKARI* coordinates.

2.2. Observations and data reduction

We used AAOmega, the fibre-fed optical spectrograph (Sharp et al. 2006) at the Anglo Australian Observatory to obtain optical spectra of our targets. Observations were made in 2007/08 as shown in Table 1. Gratings were 385R and 580V with central wavelengths 7250Å and 4800Å, and wavelength resolution $\lambda/\Delta\lambda$=1300. We successfully obtained 1,492 spectra.

The spectra were reduced using the standard AAOmega pipeline 2dfdr data reduction software (Croom et al. 2004). The combined spectra have a range of about 3800 - 8800Å. We used IRAF routine ONEDSPEC/SPLOT to identify redshifts. We also wrote a graphic user interface (GUI) in IDL in order to visually inspect the spectra by moving emission line templates across the spectra, and also to identify local lines and artefacts present in the data. As described in Sedgwick et al. (2011), we found several local artefacts in many of the spectra, often relating to neon emission from street lighting in a nearby town and identified these in our GUI to avoid false identifications.

3. RESULTS

3.1. Redshift identifications

The redshifts identified by atomic emission lines fall into three bands (see Table 1). The largest number of sources were found at $z \leq 0.345$ and could be identified by their Hα λ6563 line, which fell into our spectral range at this redshift. The nearby [NII] $\lambda\lambda$6548, 6583 lines were usually also observed, as was the [SII] doublet $\lambda\lambda$6716, 6731 unless it was redshifted out of range.

Secondly, sources at $0.345 < z \leq 1.0$, for which the strongest observable lines are the three Hβ/[OIII]/ [OIII] $\lambda\lambda$4861, 4958, 5007 emission lines (up to about $z = 0.74$). Redshifts were taken only where there was

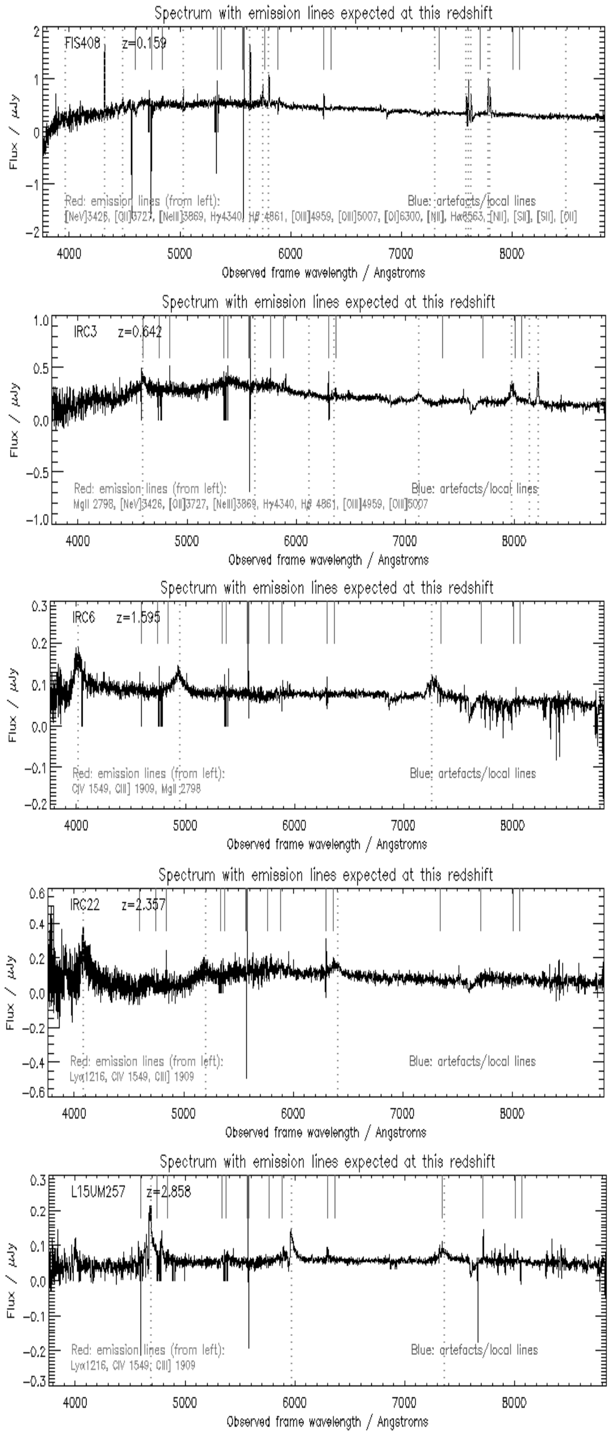

Figure 2. Examples of three spectra at different redshifts and the two detections from Lyα lines. The potential emission lines at this redshift are full-length dotted lines; the local artefacts are short solid lines from top of spectra (shown in colour online). Flux is subject to final calibration. From top: (a) FIS408, redshift $z = 0.179$, from Oct-07 fibre 22. (b) IRC3, $z = 0.642$, Oct-07 fibre 133. (c) IRC6, redshift $z = 1.595$, Jan-08 fibre 122 (all unsmoothed). (d) IRC22 at redshift $z = 2.357$ Oct-07 fibre 59 (boxcar smoothed, 3 pixels); relative fluxes of the three peaks should be 100:63:29 (Francis et al. 1991). (e) L15UM257 at $z = 2.858$, Jan-08 fibre 265 (unsmoothed).

Table 2
Redshift detection of sources catalogue.

Source	Wave-length μm	Total no. observed	Distinct Sources Observed	Redshifts identified No.	%
IRC	15	584	522	75	14%
IRC	24	319	157	82	52%
FIS	90	392	319	190	60%
BLAST	250-500	162	155	50	32%
AzTEC	1100	21	12	7	58%
Other		14	11	0	
Total		1,492	1,176	404	34%

evidence for these three emission lines. In addition, the asymmetrical [OII] emission line resulting from the close doublet $\lambda\lambda$ 3726, 3729 was often found at the same redshift to support the identifications.

Thirdly, after a gap in the redshift range without strong emission lines, there is a possibility of identifying several broad emission lines at redshifts $z > 1$. At about $1.0 < z < 1.7$ two strong lines are available: CIII] λ1909 and MgII λ2798. Above $z \sim 2.3$, Lyα λ1216 comes into range, and up to $z \sim 3$ this can be supported by CIV λ1549 and CIII] λ1909.

A total of 404 redshifts were measured for the 1,492 sources targeted (see Table 1). Examples of spectra obtained showing the redshift identifications in these three regions, and the spectra with the two highest redshifts, are given in Figure 2.

3.2. *Flux calibration of spectra*

The AAOmega spectra were not calibrated (this part of the reduction pipeline was not in place, and no flux calibration data were observed on the five nights). To enable calibration, we are using broadband photometric data from the LaSilla/WFI R-band catalogue for the field (Baronchelli et al., in prep). Choosing sources at $z < 0.1$ so that the H-alpha emission line falls within the high-throughput region of the WFI filter, and applying the AAOmega grating throughputs and WFI R-band filter, we integrate the AAOmega counts over the WFI broadband region and compare the result to the WFI flux. When results are finalised, we anticipate providing line luminosities for all observed lines.

4. DISCUSSION

4.1. *Luminosity function*

An earlier paper (Sedgwick et al. 2011) used 130 of these spectroscopic-redshift sources to prepare a luminosity function of star-forming galaxies selected at 90 μm at $0 < z < 0.25$. The result agreed well with a prediction by Serjeant & Harrison (2005), and also with predictions from a model by Gruppioni et al. (2011).

4.2. *Proportions AGNs and LIRGs*

For the 320 sources at $z \leq 0.345$, the FWHM of the Hα lines showed only two sources over 1000 km s^{-1}, and the majority under 500 km s^{-1}, suggesting few of these sources are dominated by AGN emission. Another method for discriminating between AGNs and star-forming galaxies (SFGs) is the BPT diagram (Baldwin et al. 1981), shown in Figure 3 (top). This shows a minority ($\sim$13%) of sources dominated by AGN, with a significant fraction in the intermediate region showing evidence of both SFGs and AGNs. This is broadly consistent with previous results e.g. Manners et al. (2004), who found 19% for 15 μm-selected sources and Caputi et al. (2007), who found 17% for 24 μm-selected sources.

4.3. *Star formation rates and Balmer decrement*

Star formation rates over $\sim 10^3$ M$_\odot$yr^{-1} were found for higher-redshift sources; local galaxies were typically $\leq$20 M$_\odot$yr^{-1} (see Fig. 3, middle). The Balmer decrement Hα/Hβ is shown in Fig. 3 (bottom) for sources at $z <$ 0.345. This shows very slight increase with redshift, and a median decrement of 5.9 with a large scatter.

4.4. *Multi-wavelength data for spec-z sources*

Multi-wavelength data already available for the ADF-S include *AKARI*-FIS (Shirahata et al. in prep.), *AKARI*-IRC (Davidge et al. in prep.), *Spitzer*-MIPS (Clements et al. 2011; Scott et al. 2010), BLAST (Valiante et al. 2010), *Herschel*-SPIRE (HerMES DR2; Oliver et al. 2012), submillimetre ASTE/AzTEC (Hatsukade et al. 2011) and radio ATCA (White et al. 2012) as well as studies matching *AKARI* to public data (Malek et al. 2010, 2014). Data will soon be available for *Spitzer*-IRAC (Baronchelli et al. in prep.), *Herschel*-PACS (Hatsukade et al. in prep.; HerMES), and optical and NIR data from CTIO, WFI, VST and VISTA in the UBVIRgizYJHK$_S$ bands. The optical and NIR will enable SED template fitting to our spectroscopic sources, so that further properties including age, mass, metallicity and extinction may be estimated for our sources.

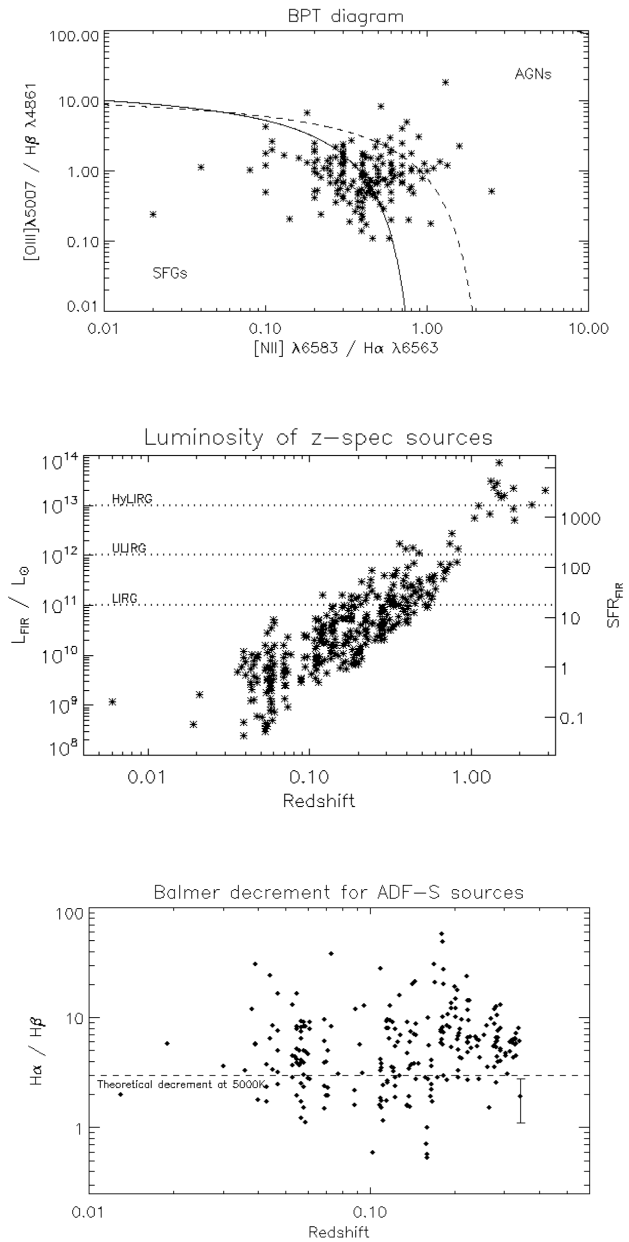

Figure 3. Top: BPT diagram for the 192 sources for which the two ratios have been determined by the AAOmega spectroscopy. The area between the solid line (Kauffmann et al. (2003)) and the dashed line (Kewley et al. (2006)) indicates composite AGN-SFG sources. Middle: Plot of FIR luminosity and SFR based on L$_{\rm FIR}$ for sources detected at 24 μm by *Spitzer*-MIPS in ADF-S. L$_{\rm FIR}$ was estimated using the M82 SED, and SFR (right-hand axis) was estimated from this using the Kennicutt (1998) formula. Bottom: The Balmer decrement for sources at $z <$ 0.345. Note indicative error bar on right of figure.

ACKNOWLEDGMENTS

This research is based on observations with *AKARI*, a JAXA project with the participation of ESA. This work was funded in part by STFC (grant PP/D002400/1), the Royal Society (2006/R4-IJP), the Sasakawa Foundation (3108) and KAKENHI (19540250 and 21111004).

REFERENCES

Baldwin, J. A. et al., 1981, Classification parameters for emission-line spectra of extragalactic objects, PASP, 93, 5

Caputi, K. I. et al., 2007, Infrared luminosity function of galaxies at z=1 and z∼2 in GOODS Fields, ApJ, 660,97

Clements, D. L. et al., 2011, ADF-S: Spitzer 24- and 70-μm observations, catalogues and counts, MNRAS, 411, 373

Croom, S., 2004, 2dfdr Overhaul, AAONw, 106, 12

Francis, P. J. et al., 1991, A high signal-to-noise ratio composite quasar spectrum, ApJ, 373, 465

Gruppioni, C. et al., 2011, Modelling galaxy and AGN evolution in the infrared, MNRAS, 416, 70

Hatsukade, B. et al., 2011, AzTEC/ASTE 1.1-mm survey of the AKARI Deep Field South, MNRAS, 411, 102

Kauffmann, G. et al., 2003, The host galaxies of active galactic nuclei, MNRAS, 346, 1055

Kawada, M. et al., 2007, FIS for AKARI, PASJ, 59, 389

Kennicutt, R. C., 1998, Star formation in galaxies along the Hubble Sequence, ARA&A, 36, 189

Kewley, L. J. et al., 2006, The host galaxies and classification of active galactic nuclei, MNRAS, 372, 961

Malek, K.et al., 2010, Star forming galaxies in the AKARI Deep Field South, A&A, 514, A11

Malek, K. et al., 2014, Properties of star forming galaxies in the AKARI Deep Field-South, A&A, 562, A15

Manners, J. C. et al., 2004, Mid-infrared sources in the ELAIS deep X-ray survey, MNRAS, 355, 97

Matsuhara, H. et al., 2006, Deep extragalactic surveys around the Ecliptic Poles with AKARI, PASJ, 58, 673

Matsuura, S. et al., 2011, Detection of the Cosmic Far-infrared Background in ADF-S, ApJ, 737, 2

Murakami, H. et al., 2007, The Infrared astronomical mission AKARI, PASJ, 59, S369

Oliver, S. J., et al., 2012, The Herschel Multi-tiered Extragalactic Survey: HerMES, MNRAS, 424,1614

Onaka, T., et al. 2007, The Infrared Camera (IRC) for AKARI: design and imaging performance, PASJ, 59, 401

Scott, K. S. et al., 2010, Spitzer MIPS 24 and 70 μm Imaging near the South Ecliptic Pole, ApJS, 191, 212

Sedgwick, C. et al., 2011, Far-infrared luminosity function of local star-forming galaxies in ADF-S, MNRAS, 416, 1862

Serjeant, S. and Harrison, D., 2005, Local submillimetre luminosity functions and predictions, MNRAS, 356, 192

Sharp, R. et al., 2006, Performance of AAOmega, SPIE, 6269, E14

Valiante, E. et al., 2010, BLAST observations of the South Ecliptic Pole Field, ApJS, 191, 222

White, G. J. et al., 2012, A deep ATCA 20 cm radio survey of the AKARI Deep Field South, MNRAS, 427, 1830